JCTC Journal of Chemical Theory and Computation

Article

pubs.acs.org/JCTC

The Right Computational Recipe for Olefin Metathesis with Ru-Based Catalysts: The Whole Mechanism of Ring-Closing Olefin Metathesis

Albert Poater,*[,§] Eva Pump,[†,‡] Sai Vikrama Chaitanya Vummaleti,[‡] and Luigi Cavallo*[,‡,⊥]

[§]Institut de Química Computacional i Catàlisi and Departament de Química, Universitat de Girona, Campus Montilivi, 17071 Girona, Catalonia, Spain

[†]Institute for Chemistry and Technology of Materials, Graz University of Technology, Stremayrgasse 9, A 8010 Graz, Austria

[‡]Kaust Catalysis Center, Physical Sciences and Engineering Division, King Abdullah University of Science and Technology, Thuwal 23955-6900, Saudi Arabia

[⊥]Dipartimento di Chimica e Biologia, Università di Salerno, Via Ponte don Melillo, I-84084 Fisciano (SA), Italy

Supporting Information

ABSTRACT: The initiation mechanism of ruthenium methylidene complexes was studied detailing mechanistic insights of all involved reaction steps within a classical olefin metathesis pathway. Computational studies reached a good agreement with the rarely available experimental data and even enabled to complement them. As a result, a highly accurate computational and rather cheap recipe is presented; M06/TZVP//BP86/SVP (PCM, P = 1354 atm).

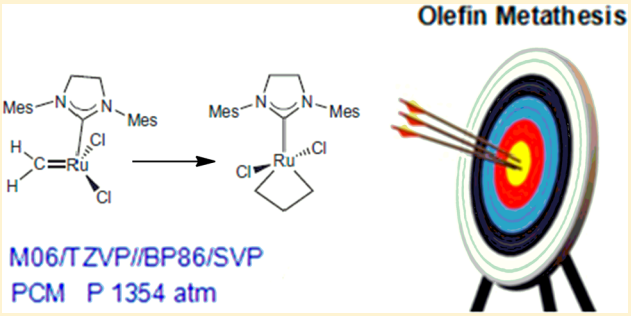

INTRODUCTION

Understanding the reaction mechanisms that lead to the formation of desired products is the key for developing better catalysts. In the field of olefin metathesis,[1] Chauvin proposed already in the 1970s that the active catalyst was a metal−carbene complex and that the respective four-membered ring metallacycle derivatives are leading to the formation of the desired products.[1c,2] This discovery paved the route to the design of well-defined catalysts by Schrock and Grubbs, and transformed olefin metathesis into one of the most important tools for the formation of carbon−carbon bonds in modern synthetic chemistry. The first experimental[3] and theoretical insights[4] in regard to the mechanism were achieved since the late 1990s. In general, the accepted mechanism of olefin metathesis for Ru first and second generation catalysts can be divided into three parts: initiation, propagation and termination. Since these studies, Density Functional Theory (DFT) calculations have been extensively used to clarify many aspects of Ru-catalyzed olefin metathesis,[5,6] and efforts have been also been made to validate computational protocols.[7]

In this context, a detailed mechanistic work by Piers and coworkers, which unraveled the details of the kinetics of this reaction by characterizing several of the intermediates inside the catalytic cycle,[8] represents a valuable opportunity to check for the performance of DFT methods. In detail, Piers and coworkers characterized the key steps during the ring closing metathesis (RCM) of dimethyl diallyl malonate (DMDAM) using a second generation ruthenium complex, as illustrated in Figure 1a. Such a detailed study offers the opportunity to test

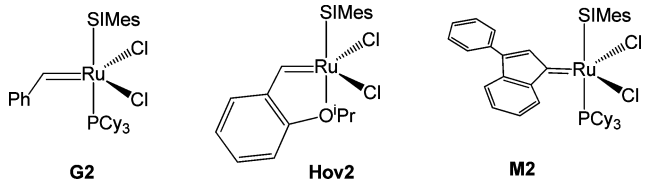

Figure 1. Chemical structures of commercially available 2nd generation catalysts (SIMes = *N*,*N*′-bis[2,4,6-(trimethyl)phenyl]-imidazolidin-2-ylidene).

the performance of standard DFT based computational protocols. Indeed, herein, we propose a computational protocol (M06/TZVP//BP86/SVP (PCM, P = 1354 atm)) to deal with Ru-based olefin metathesis catalysts. Although not expensive, the proposed method works with high precision, offering a computationally effective tool for rationalizing experimental available data, as well as a prediction of the behavior of the catalyst.

COMPUTATIONAL DETAILS

All the DFT static calculations were performed with the Gaussian 09 set of programs.[9] The electronic configuration of the molecular systems was described with the standard split-valence basis set with a polarization function of Ahlrichs and coworkers for H, C, N, and Cl (SVP keyword in Gaussian).[10] For

Received: May 4, 2014
Published: August 25, 2014

   dx.doi.org/10.1021/ct5003863 | *J. Chem. Theory Comput.* 2014, 10, 4442−4448

Ru, we used the small-core, quasi-relativistic Stuttgart/Dresden effective core potential, with an associated valence basis set contracted (standard SDD keywords in Gaussian 09).[11] The geometry optimizations were performed without symmetry constraints, and the characterization of the located stationary points was performed by analytical frequency calculations. Only two functionals, BP86 and M06, were used in the geometry optimization: the first corresponding to a well-established and computationally fast GGA functional, the second corresponding to one of the last generation HMGGA functionals, at the other side of the Jacob ladder.

A larger number of functionals were tested through single point energy calculations on the BP86 geometries with using the triple-ζ valence plus polarization basis set for main group atoms (TZVP keyword in Gaussian). Solvent effects were included with the polarizable continuous solvation model PCM using CH_2Cl_2 as solvent.[12] Since entropic contribution calculated within the ideal gas approximation at P = 1 atm is likely exaggerating the expected values for the dissociative steps in the condensed phase,[13,14] all the thermochemical analysis was performed at P = 1354 atm and T = 298.15 K, as suggested by Martin et al.[15]

The Supporting Information file includes the Cartesian coordinates and energies of all species discussed in this work.

RESULTS

Before discussing our results, we briefly recall that Piers and coworkers succeeded in characterizing energy barriers and relative energies between the 14e species **1**, the coordination intermediate **4** and as well as the other important ruthenacyclobutene derivates **2**, **3**, and **5** by kinetic and thermodynamic experiments, carried out by low temperature NMR spectroscopic experiments or mass spectrometry studies.[16] The discussed structures and labels can be found in Scheme 1b.

Scheme 1. (a) Typical Benchmark RCM Reaction with Ru Based Catalyst and Dimethyl Diallyl Malonate (DMDAM) Substrate. (b) Experimentally Observed Key Intermediates for Ring Closing Metathesis Pathway Using DMDAM as a Substrate

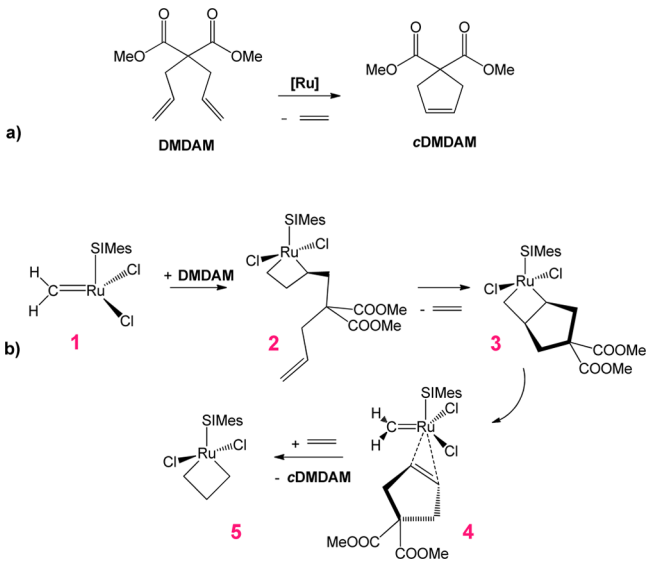

The limiting reaction step was determined to be the formation of the metallacycle **2** (**2** → **1**), which costs 66 kJ/mol. Referred to the metallacycle **3**, this means that the ring opening step (**3** → **1**) is 70 kJ/mol more expensive than the ring closing step (**3** → **5**), costing 5 kJ/mol less. Detailed energy values can be found in Table 1, entry 1. With these results in hand, we tested a set of computational methods to reproduce the experimentally available data, as shown in Table 1, entries 2−42. Going into the detail, using BP86 and B3LYP functionals results in a bad description of binding energy, which is the energy required for the **3** → **1** step (entries 8, 13, and 16). This observation is in line with previous studies indicating that proper description of dispersion interactions is mandatory to obtain absolute reaction energies of ruthenium and ligand binding.[7a−e,17,18] Indeed, with these old functionals better agreement with the experiments can be achieved by considering the simple ΔE, since the error in the binding energy is compensated by a similar error when entropic contributions are neglected. Next, results with the PBE and PBE1PBE functionals are substantially in line with those obtained using BP86 and B3LYP functionals. Moving to MGGA functionals, the effect is the opposite: it achieves a good balance for the ΔG, either using the pure M06L (entry 22) and, particularly, the hybrid M06 functional (entry 6). As a simple test on the impact of the functional used for geometry optimizations, we compared results obtained with the simplest GGA BP86 functional[19] with those obtained with the more modern and complex MHGGA M06 functional, with the conclusion that the cheaper BP86 functional performs well (compare entries 6 and 9). The influence of the basis set (SVP and TZVP) on the quality of the results in gas phase calculations was investigated in combination with both (BP86 and M06) functionals. The more expensive TZVP leads to a better agreement in M06 geometry optimizations (entries 9 and 11), while better agreement is achieved with the SVP basis set in case of the BP86 functional (entries 6 and 32). Focusing on the solvation models, the PCM model gives marginal better agreement with experiments relative to the recently developed SMD model (comparing entries 6 and 29), although for the PCM model better agreement is found if nonelectrostatic terms (repulsion, cavitation, and dispersion) are neglected (entries 6 and 31). Results obtained when adding an empirical term to take into account the dispersion effects are collected in entries 16, 20, and 34. In the frame of the model used here (functional, basis set, solvent) no clear improvement was achieved by using HGGA instead of classical GGA functionals (compare also entries 13 and 16).[19] Differently, the M06 family of functionals, which were tuned to reproduce a data set including also dispersion dominated systems,[20] results in an overall good description of the experimental results. On the other hand, in entries 35−38 the inclusion of the dispersion on the geometry optimizations turned out to give less reproducibility with respect to the experimental data.[21] To sum up, this means that the inclusion of dispersion during the optimization process leads to worse results, but its addition in single point energy calculations on top of a BP86/SVP optimization improves the accuracy, which might occur due to some error compensations. The use of diffuse basis sets on Cl and O atoms in entries 39−41 does not improve the results either, and in entry 42 the effect of modifying the pressure in the thermochemical analysis, to better simulate the liquid conditions, helps to reach the right description of the interaction between different moieties.[14a,16] Indeed, the increase of the pressure turns out to give better

dx.doi.org/10.1021/ct5003863 | J. Chem. Theory Comput. 2014, 10, 4442−4448

Table 1. Comparison between Experimental Energies and the Values Obtained Using Different Computational Methods for the Ring Closing Metathesis Reaction Pathway Considering Complex 5 as a Reference[a]

entry	method (functional(solv)/basis set) //functional(gas)/basis set)	2 → 1	3 → 2	3 with respect to 2	5 with respect to 3	3 → 4	3 → 1	4 → 4′	MUE
1	$\Delta G_{exp.}$	66	63	−4	−10	55	65	55	
2	ΔE (gas) BP86/SVP	113	73	19	−15	66	70	69	16
3	ΔG (gas) BP86/SVP	81	65	−39	−23	63	72	61	12
4	ΔG (gas, P = 1354 atm) BP86/SVP	81	69	−22	−23	63	72	61	10
5	ΔE (pcm) M06/TZVP//BP86/SVP	100	65	33	−2	58	59	60	14
6	ΔG (pcm) M06/TZVP//BP86/SVP	68	57	−26	−10	55	61	53	5
7	ΔE BP86/TZVP//BP86/SVP	70	64	1	−21	57	73	65	6
8	ΔG (pcm) BP86/TZVP//BP86/SVP	38	56	−58	−29	53	76	57	18
9	ΔG (pcm) M06/TZVP//M06/SVP	58	58	−18	16	56	47	54	10
10	ΔE (pcm) M06/TZVP//M06/TZVP	87	72	35	1	57	61	65	14
11	ΔG (pcm) M06/TZVP//M06/TZVP	70	67	−19	−11	49	55	53	6
12	ΔE (pcm) B3LYP/TZVP//BP86/SVP	46	45	4	−22	49	73	57	11
13	ΔG (pcm) B3LYP/TZVP//BP86/SVP	13	36	−55	−30	45	75	50	25
14	ΔG (pcm, P = 1354 atm) B3LYP/TZVP//BP86/SVP	14	40	−38	−30	45	75	50	22
15	ΔE (pcm) B3LYP-D3/TZVP//BP86/SVP	65	23	39	9	45	35	37	23
16	ΔG (pcm) B3LYP-D3/TZVP//BP86/SVP	32	14	−20	1	42	38	30	25
17	ΔE (pcm) B3PW91/TZVP//BP86/SVP	72	76	−3	−23	60	87	76	12
18	ΔG (pcm) B3PW91/TZVP//BP86/SVP	40	67	−61	−31	56	90	69	21
19	ΔE (pcm) B97D/TZVP//BP86/SVP	67	29	31	14	46	44	47	19
20	ΔG (pcm) B97D/TZVP//BP86/SVP	35	21	−28	7	43	46	40	23
21	ΔE (pcm) M06L/TZVP//BP86/SVP	90	51	30	−5	59	49	50	14
22	ΔG (pcm) M06L/TZVP//BP86/SVP	58	43	−29	−13	55	51	43	12
23	ΔE (pcm) PBEBPE/TZVP//BP86/SVP	83	69	13	−19	61	75	69	11
24	ΔG (pcm) PBEBPE/TZVP//BP86/SVP	51	60	−46	−26	58	78	62	14
25	ΔE (pcm) PBE1PBE/TZVP//BP86/SVP	92	85	12	−19	64	88	82	19
26	ΔG (pcm) PBE1PBE/TZVP//BP86/SVP	59	77	−47	−27	60	91	75	19
27	ΔE (pcm) PBEh1PBE/TZVP//BP86/SVP	91	83	13	−18	62	85	79	17
28	ΔG (pcm) PBEh1PBE/TZVP//BP86/SVP	58	74	−46	−26	59	88	72	17
29	ΔG (smd) M06/TZVP//BP86/SVP	63	63	−28	−17	58	74	66	8
30	ΔG (smd, P = 1354 atm) M06/TZVP//BP86/SVP	63	67	−11	−17	58	74	66	6
31	ΔG (pcm, nonelectrostatic terms) M06/TZVP//BP86/SVP	80	64	−28	−20	51	49	47	11
32	ΔE (pcm) M06/TZVP//BP86/TZVP	108	65	31	−3	57	57	59	14
33	ΔG (pcm, P = 1354 atm) M06/TZVP//BP86/TZVP	68	51	−1	−7	49	55	46	6
34	$\Delta\Delta G$ (gas) BP86-D3/SVP	19	−22	35	31	−3	−37	−20	64
35	ΔE (pcm, P = 1354 atm) M06/TZVP//BP86-d3/SVP	47	77	37	4	62	63	69	16
36	ΔG (pcm, P = 1354 atm) M06/TZVP//BP86-d3/SVP	46	72	5	−18	54	56	53	8
37	ΔG (pcm, P = 1354 atm) M06/TZVP//B3LYP-d3/SVP	44	76	35	4	61	61	4	21
38	ΔG (pcm, P = 1354 atm) M06/TZVP//B3LYP-d3/SVP	38	74	−6	−10	58	54	58	8
39	ΔE (pcm) M06/TZVP(diffuse on Cl and O)//BP86/SVP	98	63	32	−4	58	59	58	12
40	ΔG (pcm) M06/TZVP(diffuse on Cl and O)//BP86/SVP	66	54	−27	−12	54	61	51	6
41	ΔG (pcm, P = 1354 atm)) M06/TZVP(diffuse on Cl and O)// BP86/SVP	65	58	−9	−12	55	61	51	3
42	ΔG (pcm, P = 1354 atm) M06/TZVP//BP86/SVP	68	61	−8	−10	55	61	53	2

[a]The given energies are in kJ/mol. MUE is the mean unsigned error between the experimental and the calculated energy values.

results in all protocols, as can be exemplary read out from entries 13 and 14, 29 and 30, as well as 6 and 42.

Overall, the best agreement with the small data set of experimental free energies is achieved with the protocol of entry 42. In this case, the MUE amounts only 2 kJ/mol, although it is not clear if also experimentally gained values are subjected to errors of some kJ/mol. A slightly higher MUE of around 5−8 kJ/mol is achieved with the protocols of entries 6, 11, 29, 33, and 36. Considering the errors inherent in the experimental data, the protocols above can be considered as equivalent. All other protocols to evaluate ΔG result in MUEs greater than 10 kJ/mol. This indicates that the best protocols, in terms of agreement with the experimental results and computational efficiency, correspond to single point energy calculations at the M06 level, with a relatively good quality basis set such as the TZVP basis set, on BP86 optimized geometries optimized with the lower quality SVP basis set.

A tuning of the final ΔG can be achieved by selecting a specific solvation model or a pressure different from 1 atm in the thermochemical analysis. Overall, this is a computationally convenient protocol, since GGA functionals are remarkably faster than MHGGA functionals. As an overall comment, it should be noted that, with a few exceptions, basically all the protocols we tested result in MUE between 10 and 20 kJ/mol. This confirms the robustness of the most typical functionals in describing transition metal promoted reactivity. On the other hand, bearing in mind attempts with truncated catalytic models with the most expensive CCSD(T) calculations,[22] the latter

dx.doi.org/10.1021/ct5003863 | J. Chem. Theory Comput. 2014, 10, 4442−4448

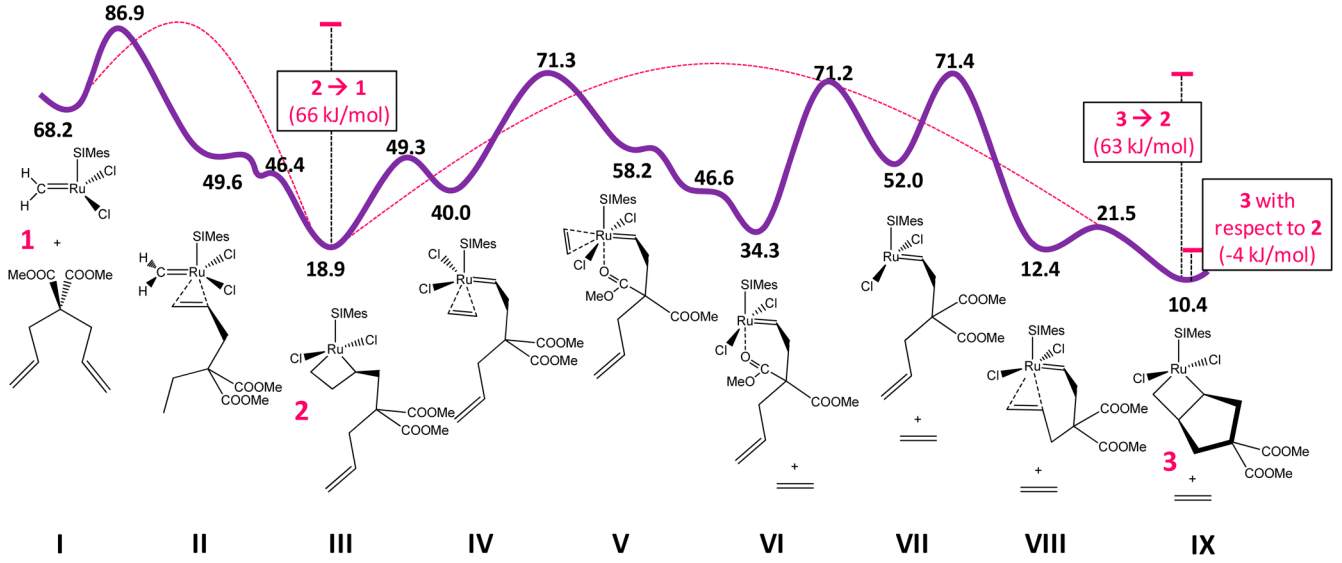

Figure 2. Computed stationary points for the reversed ring opening metathesis pathway using DMDAM as a substrate. The given free energies (in kJ/mol) are with respect to the reference complex **5**. All reaction intermediates are presented exemplary; experimentally observed complexes are labeled with numbers (in red).

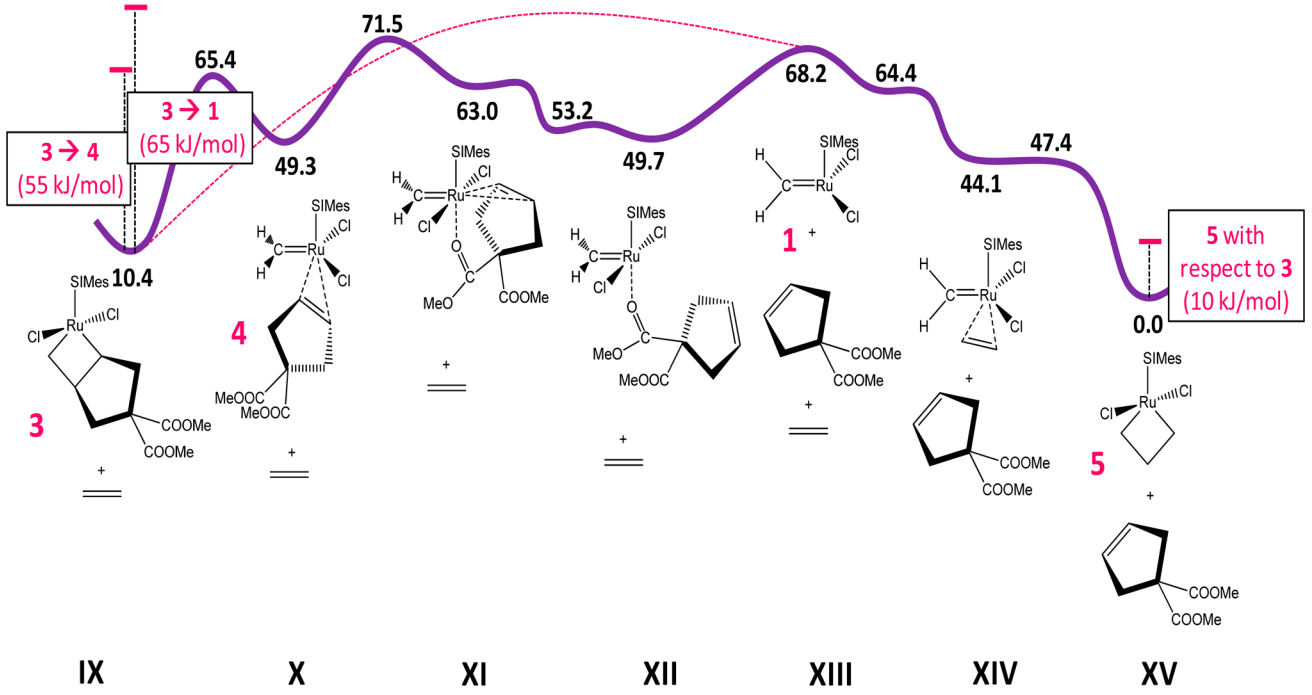

Figure 3. Computed stationary points for the ring closing metathesis cycle. The given free energies (in kJ/mol) are with respect to the reference complex **5**. All reaction intermediates are presented exemplary; experimentally observed complexes are labeled with numbers (in red).

method as well as MP2 are still unaffordable for mechanistic studies with real catalysts and real substrates. However, the proposed DFT approach here reaches a good agreement with experimental data yet. Finally, we remark that the approach we propose, medium level for geometry optimizations, and increasing the level for single point energy calculations, is similar to the approach used by Houk et al. in investigating Ru-catalyzed olefin metathesis, based on the B3LYP functional for geometry optimization, and the M06 functional for final energy calculations.[23,24]

Having established that the best protocol corresponds to entry 42, in the following, we applied it to compose the overall computational reaction pathway (**I** → **XV**), thus filling the energy values experimentally not available. For better clarity, we divided the studied pathway into a reversed ring opening (**I** → **IX**, Figure 2) and a ring closing metathesis cycle (**IX** → **XV**, Figure 3). Starting from the 14e species **1**, the first step (**I**–**II**) corresponds to the coordination of a free olefin substrate, DMDAM, trans to the SIMes group of the catalyst, which results in the formation of intermediate **II**. This step requires the rotation of the ylidene group of the catalyst which provides the space for the entering olefin to interact with Ru metal. From a thermodynamic point of view, the substrate bound intermediate **II** is 18.6 kJ/mol below the species 1. It requires

dx.doi.org/10.1021/ct5003863 | J. Chem. Theory Comput. 2014, 10, 4442−4448

18.7 kJ/mol to overcome the upper energy point (**I**−**II** at 86.9 kJ/mol) for the reaction path, as shown in Figure 2. Next, intermediate **II** readily collapses in the more stable and experimentally detected metallacycle **2** (**III**), which lies 49.3 kJ/mol below the species **1**. This step is predicted to be barrierless. To sum up this part, our results clearly suggest that the experimentally described **2** → **1** transition energy (or **III**−**I** in Figure 2) is equivalent to the predicted upper barrier placed at 86.9 kJ/mol and corresponds to the transition state **I**−**II**. In other words, a barrier of 68.0 kJ/mol must be overcome to go from **III** to **I** (since intermediate **III** is placed at 18.9 kcal/mol), which is in good agreement with the experimental value of 66 kJ/mol.

This not meaningless step **III** → **IV** was treated in previous studies with simple ethylenes instead of real alkene substrates. However, recent work of Plenio,[25] Blechert,[26] and Solans-Monfort[27] focused on describing this step.

To go from **2** → **3** (**III**−**IX** in Figure 2), we located all different possible intermediates. Going into detail, ring opening of metallacycle **III** results in the formation of coordination intermediate **IV**, which lies 21.1 kJ/mol above **III** and requires the overcoming of an energy barrier of 30.4 kJ/mol. The next step corresponds to the haptotropic shift in **IV** that leads to isomer **V**, in which one of the methyl carboxylic groups of the substrate coordinates to Ru metal via O atom trans to the SIMes ligand by displacing the ethylene molecule cis to the SIMes. This step proceeds through transition state **IV**−**V** and requires to overcome a barrier of 31.3 kJ/mol. Then, the removal of the ethylene molecule from **V** leads to the formation of intermediate **VI**, which lies 23.9 kJ/mol below **V**. This step is predicted to be barrieless suggesting that the dissociation step involving small olefins are kinetically meaningless. We point out that the dissociation of ethylene could take place directly from species **IV**. However, all attempts to get the corresponding transition state collapsed in a structure with a direct Ru−O interaction that stabilizes the sphere of the ruthenium. Indeed, formation of a Ru−O bond allows the release of the olefin from the metal to be exothermic, gaining an energy amount of 24.1 kJ/mol from **V**. Furthermore, the release of the olefin is thought to be sometimes the upper barrier in olefin metathesis as Plenio or Solans-Monfort have been recently announced,[25,27] which is confirmed by the barrier of the first step **II** → **I** asks for 37.3 kJ/mol for the dissociation of the olefin, which is not that low, whereas the upper barrier for **IV** → **VII** is only slightly lower, being 31.3 kJ/mol.

The next step corresponds to the cleavage of the Ru−O bond leading to less stable 14e intermediate **VII** (17.7 kJ/mol above **VI**) with a vacant coordination site trans to SIMes. From a kinetic point of view, this step **VI** → **VII** is the most expensive of the **I** → **IX** pathway requiring 36.9 kJ/mol. The generation of this second 14e species (**VII**) brings along a free site on the metal center. Then, the vacant coordination site on **VII** is occupied by the terminal alkene group of the ylidene ligand to form intermediate **VIII**. The predicted barrier of 19.4 kJ/mol for this step is comparable to the DMDAM substrate coordination barrier (**I**−**II**), differing only by 0.7 kJ/mol. Finally, intermediate **VIII** collapses readily in the stable metallacycle **3** (**IX**). This is a rather low energy step with a barrier of only 9.1 kJ/mol. It is worth mentioning here that, from a thermodynamic point of view, the experimentally determined metallacycle **3** was found to be around 4.0 kJ/mol more stable than **2** whereas our calculations predicted a slightly more stable **3** (8.5 kJ/mol than **2**). Furthermore, similar to **2** → **1** transition, our predicted barriers are within experimental accuracy for the **3** → **2** transition (**IX** → **III** in Figure 2). For instance, the computed barrier for the step **IX** → **III** is 60.9 kJ/mol, which is comparable to the experimental value of 63.0 kJ/mol. These small energy discrepancies are insignificant when taking into account the error of the computational methods.

Moving to the second part **IX**−**XV** of the RCM mechanism (see Figure 3), we first considered the opening of the metallacycle **3** (**IX**) to form coordination intermediate **4** (**X**). This step requires the overcoming of a barrier (**IX**−**X**) of 55 kJ/mol, which is identical to the experimental barrier value of 55.0 kJ/mol. The next experimentally observed step (**4** → **1**) involves computationally two more intermediates **XI** and **XII**. The structural rearrangement of **X** leads to a less stable intermediate **XI** (13.7 kJ/mol above **X**), through rotation of the coordinated *c*DMDAM from trans to cis with respect to the SIMes. The concomitant destabilization in this step is partly compensated by a favorable intramolecular interaction of the Ru metal with a carbonyl group of the pentene derivative. In the next step, the interaction between the double bond of the product cDMDAM and ruthenium breaks leading to intermediate **XII**, which lies 13.3 kJ/mol below **XI**. This step is predicted to be barrier less. From a structural point of view, intermediate **XII** coordinates to product *c*DMDAM via Ru−O bond. The penultimate step corresponds to the product *c*DMDAM release from **XII**, leading to the formation of the less stable 14e species **1** (**XIII** in Figure 3). From a thermodynamic point of view, species **1** lies 18.5 kJ/mol above **XII**. Since we were not able to locate the barrier for the **XIII**−**XIV** transition, it will be treated as a quasi-dissociative step that completely releases the pentene derivative.

The final step includes the coordination of an ethylene molecule trans to SIMes (**XIV**) followed by a collapse of the system to metallacycle **5** (**XV**). Overall, from the studied RCM reaction pathway (**IX** → **XV**), we may draw two important conclusions corresponds to the experimental data. First, the predicted upper barrier for **3** → **5** transition is 61.1 kJ/mol, which is in reasonably good agreement with the experimental value (65.0 kJ/mol). Secondly, our results suggest that the thermodynamic equilibrium between complexes **3** and **5** is placed 10.4 kJ/mol in favor of complex **5**, which is almost similar to the experimental value of 10.4 kJ/mol.

Having completed the description of the whole catalytic cycle, next we turn to address the rotation of the methylidene-hydrogens of complex **4** (see Scheme 2) studied by Piers and co-workers. In **4**, a 180° rotation around the Ru=CH_2 bond should occur easily through a transition state **4**−**4′**, where the methylidene is nearly prependicular to the cyclopentene ring. Hence, this transformation is expected to proceed almost equally fast in both directions. This suggests that moving from

Scheme 2. Proposed Mechanism for Exchange of Hα′ and Hα″

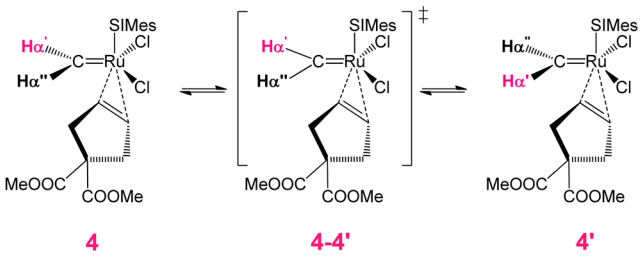

dx.doi.org/10.1021/ct5003863 | J. Chem. Theory Comput. 2014, 10, 4442−4448

3 to 4 and then rotating Hα′ and Hα″ we end up in the symmetrical 4′ and 3′, respectively, where the positions of both hydrogen atoms are exchanged. Most importantly, the predicted barrier (4−4′) of 52.9 kJ/mol is in good agreement with the experimental value of 55 kJ/mol.

CONCLUSIONS

The take-home message of the present study is that among all computational protocols we tested for modeling the reactivity promoted by transition metal complexes, most of the generally used approaches performed reasonably well with MUEs from experimentally determined free energies below 20 kJ/mol. Notwithstanding, some of the computational approaches based on the M06 functionals for the calculations of the energy result in a high agreement with available experimental data. Interestingly, the impact of the basis set and of the functional on the geometry optimization is marginal, which allows using the computationally convenient combination of the cheaper BP86 functional and SVP basis set in the geometry optimizations in gas phase, and only moving to the more expensive M06 functional in combination with the TZVP basis set for single point energy calculations in solvent (Mo6/TZVP//BP86/SVP). The various PCM solvation models we tested perform similarly in the present case. A thermodynamic analysis was performed at a pressure of 1354 atm, to better reflect the liquid phase used experimentally. Consequently, a better agreement with the experiments was found ascribed to a more balanced evaluation of the entropic term in the coordination/dissociation of the substrate from the metal center. Based on the better performing protocol, Mo6/TZVP//BP86/SVP (PCM, P = 1354 atm), we characterized the whole ring closing metathesis (RCM) pathway for the transformation of dimethyl diallyl malonate to its cyclic pentene derivative, by filling the numbers that was impossible to measure experimentally, offering thus a complete understanding of the RCM reaction profile. As a final note, we observed a reasonably good agreement between our theoretical predictions of reaction and barrier free energies and experimental results with an error margin from 1 to 5 kJ/mol.

ASSOCIATED CONTENT

Supporting Information

Cartesian coordinates and energies of all the species discussed in this work. This material is available free of charge via the Internet at http://pubs.acs.org.

AUTHOR INFORMATION

Corresponding Authors

*Email: albert.poater@udg.edu.

*Email: luigi.cavallo@kaust.edu.sa.

Author Contributions

The manuscript was written through contributions of all authors. All authors have given approval to the final version of the manuscript.

Notes

The authors declare no competing financial interest.

ACKNOWLEDGMENTS

A.P. thanks the Spanish MINECO for a Ramón y Cajal contract (RYC-2009-05226) and European Commission for a Career Integration Grant (CIG09-GA-2011-293900). E.P. gratefully acknowledges the receipt of the "Chemical Monthly Fellowship" financed by Springer Verlag, the Austrian Academy of Sciences (ÖAW), and the Gesellschaft Österreichischer Chemiker (GÖCH).

ABBREVIATIONS

SIMes, 1,3-bis(2,4,6-trimethylphenyl)-4,5-dihydroimidazolin-2-ylidene; DMDAM, dimethyl diallyl malonate

REFERENCES

(1) (a) Chauvin, Y. *Angew. Chem., Int. Ed.* **2006**, *45*, 3740−3747. (b) Grubbs, R. H. *Angew. Chem., Int. Ed.* **2006**, *45*, 3760−3765. (c) Schrock, R. R. *Angew. Chem., Int. Ed.* **2006**, *45*, 3748−3759.

(2) Hérisson, J. L.; Chauvin, Y. *Makromol. Chem.* **1971**, *141*, 161−176.

(3) (a) Dias, E. L.; Nguyen, S. T.; Grubbs, R. H. *J. Am. Chem. Soc.* **1997**, *119*, 3887−3897. (b) Sanford, M. S.; Ulman, M.; Grubbs, R. H. *J. Am. Chem. Soc.* **2001**, *123*, 749−750. (c) Sanford, M. S.; Love, J. A.; Grubbs, R. H. *J. Am. Chem. Soc.* **2001**, *123*, 6543−6554. (d) Adlhart, C.; Hinderling, C.; Baumann, H.; Chen, P. *J. Am. Chem. Soc.* **2000**, *122*, 8204−8214. (e) Adlhart, C.; Chen, P. *Helv. Chim. Acta* **2000**, *83*, 2192−2196.

(4) (a) Vyboishchikov, S. E.; Bühl, M.; Thiel, W. *Chem.—Eur. J.* **2002**, *8*, 3962−3975. (b) Cavallo, L. *J. Am. Chem. Soc.* **2002**, *124*, 8965−8973. (c) Aagaard, O. M.; Meier, R. J.; Buda, F. *J. Am. Chem. Soc.* **1998**, *120*, 7174−7182. (d) Bernardi, F.; Bottoni, A.; Miscione, G. P. *Organometallics* **2000**, *19*, 5529−5532. (e) Adlhart, C.; Chen, P. *Angew. Chem., Int. Ed.* **2002**, *41*, 4484−4487.

(5) (a) Stewart, I. C.; Benitez, D.; O'Leary, D. J.; Tkatchouk, E.; Day, M. W.; Goddard, W. A.; Grubbs, R. H. *J. Am. Chem. Soc.* **2009**, *131*, 1931−1938. (b) van Rensburg, W. J.; Steynberg, P. J.; Meyer, W. H.; Kirk, M. M.; Forman, G. S. *J. Am. Chem. Soc.* **2004**, *126*, 14332−14333.

(6) (a) Correa, A.; Cavallo, L. *J. Am. Chem. Soc.* **2006**, *128*, 13352−13353. (b) Webster, C. E. *J. Am. Chem. Soc.* **2007**, *129*, 7490−7491. (c) Benitez, D.; Tkatchouk, E.; Goddard, W. A. I. *Chem. Commun.* **2008**, 6194−6196. (d) Mathew, J.; Koga, N.; Suresh, C. H. *Organometallics* **2008**, *27*, 4666−4670. (e) Barbasiewicz, M.; Szadkowska, A.; Bujok, R.; Grela, K. *Organometallics* **2006**, *25*, 3599−3604. (f) Poater, A.; Cavallo, L. *J. Mol. Catal. A: Chem.* **2010**, *324*, 75−79. (g) Poater, A.; Ragone, F.; Correa, A.; Cavallo, A. *Dalton Trans.* **2011**, *40*, 11066−11069. (h) Leitgeb, A.; Abbas, M.; Fischer, R. C.; Poater, A.; Cavallo, L.; Slugovc, C. *Catal. Sci. Technol.* **2012**, *2*, 1640−1643. (i) Falivene, L.; Poater, A.; Cazin, C. S. J.; Slugovc, C.; Cavallo, L. *Dalton Trans.* **2013**, *42*, 7312−7317. (j) Credendino, R.; Poater, A.; Ragone, F.; Cavallo, L. *Catal. Sci. Technol.* **2011**, *1*, 1287−1297. (k) Bantreil, X.; Poater, A.; Urbina-Blanco, C. A.; Bidal, Y. D.; Falivene, L.; Randall, R. A. M.; Cavallo, L.; Slawin, A. M. Z.; Cazin, C. S. J. *Organometallics* **2012**, *31*, 7415−7426. (l) Poater, A.; Bahri-Lalehac, N.; Cavallo, L. *Chem. Commun.* **2011**, *47*, 6674−6676. (m) Poater, A.; Cosenza, B.; Correa, A.; Giudice, S.; Ragone, F.; Scarano, V.; Cavallo, L. *Eur. J. Inorg. Chem.* **2009**, 1759−1766. (n) Benitez, D.; Goddard, W. A., III *J. Am. Chem. Soc.* **2005**, *127*, 12218−12219.

(7) (a) Kulkarni, A. D.; Truhlar, D. G. *J. Chem. Theory Comput.* **2011**, *7*, 2325−2332. (b) Zhao, Y.; Truhlar, D. G. *J. Chem. Theory Comput.* **2009**, *5*, 324−333. (c) Zhao, Y.; Truhlar, D. G. *Org. Lett.* **2007**, *9*, 1967−1970. (d) Zhao, Y.; Truhlar, D. G. *Chem. Phys. Lett.* **2011**, *502*, 1−13. (e) Zhao, Y.; Truhlar, D. G. *Acc. Chem. Res.* **2008**, *41*, 157−167. (f) Occhipinti, G.; Bjørsvik, H.-R.; Jensen, V. R. *J. Am. Chem. Soc.* **2006**, *128*, 6952−6954. (g) Minenkov, Y.; Singstad, A.; Occhipinti, G.; Jensen, V. R. *Dalton Trans.* **2012**, *41*, 5526−5541. (h) Tsipis, A. C.; Orpen, A. G.; Harvey, J. N. *Dalton Trans.* **2005**, 2849−2858.

(8) (a) Romero, P. E.; Piers, W. E. *J. Am. Chem. Soc.* **2007**, *129*, 1698−1704. (b) van der Eide, E. F.; Piers, W. E. *Nat. Chem.* **2010**, *2*, 571−576.

(9) Frisch, M. J.; Trucks, G. W.; Schlegel, H. B.; Scuseria, G. E.; Robb, M. A.; Cheeseman, J. R.; Scalmani, G.; Barone, V.; Mennucci, B.; Petersson, G. A.; Nakatsuji, H.; Caricato, M.; Li, X.; Hratchian, H.

P.; Izmaylov, A. F.; Bloino, J.; Zheng, G.; Sonnenberg, J. L.; Hada, M.; Ehara, M.; Toyota, K.; Fukuda, R.; Hasegawa, J.; Ishida, M.; Nakajima, T.; Honda, Y.; Kitao, O.; Nakai, H.; Vreven, T.; Montgomery, J. A., Jr.; Peralta, J. E.; Ogliaro, F.; Bearpark, M.; Heyd, J. J.; Brothers, E.; Kudin, K. N.; Staroverov, V. N.; Kobayashi, R.; Normand, J.; Raghavachari, K.; Rendell, A.; Burant, J. C.; Iyengar, S. S.; Tomasi, J.; Cossi, M.; Rega, N.; Millam, N. J.; Klene, M.; Knox, J. E.; Cross, J. B.; Bakken, V.; Adamo, C.; Jaramillo, J.; Gomperts, R.; Stratmann, R. E.; Yazyev, O.; Austin, A. J.; Cammi, R.; Pomelli, C.; Ochterski, J. W.; Martin, R. L.; Morokuma, K.; Zakrzewski, V. G.; Voth, G. A.; Salvador, P.; Dannenberg, J. J.; Dapprich, S.; Daniels, A. D.; Farkas, Ö.; Foresman, J. B.; Ortiz, J. V.; Cioslowski, J.; Fox, D. J. *Gaussian 09*, Revision D.01; Gaussian, Inc.: Wallingford, CT, 2009.

(10) Schaefer, A.; Horn, H.; Ahlrichs, R. *J. Chem. Phys.* **1992**, *97*, 2571−2577.

(11) (a) Haeusermann, U.; Dolg, M.; Stoll, H.; Preuss, H. *Mol. Phys.* **1993**, *78*, 1211−1224. (b) Kuechle, W.; Dolg, M.; Stoll, H.; Preuss, H. *J. Chem. Phys.* **1994**, *100*, 7535−7542. (c) Leininger, T.; Nicklass, A.; Stoll, H.; Dolg, M.; Schwerdtfeger, P. *J. Chem. Phys.* **1996**, *105*, 1052−1059.

(12) (a) Barone, V.; Cossi, M. *J. Phys. Chem. A* **1998**, *102*, 1995−2001. (b) Tomasi, J.; Persico, M. *Chem. Rev.* **1994**, *94*, 2027−2094.

(13) (a) Urbina-Blanco, C. A.; Poater, A.; Lebl, T.; Manzini, S.; Slawin, A. M. Z.; Cavallo, L.; Nolan, S. P. *J. Am. Chem. Soc.* **2013**, *135*, 7073−7079. (b) Rotzinger, F. P. *Chem. Rev.* **2005**, *105*, 2003−2037. (c) Cooper, J.; Ziegler, T. *Inorg. Chem.* **2002**, *41*, 6614−6622. (d) Margl, P. *Can. J. Chem.* **2009**, *87*, 891−903. (e) Solans-Monfort, X.; Copéret, C.; Eisenstein, O. *Organometallics* **2012**, *31*, 6812−6822. (f) Raynaud, C.; Daudey, J. P.; Jolibois, F.; Maron, L. *J. Phys. Chem. A* **2005**, *110*, 101−105. (g) Ardura, D.; López, R. L.; Sordo, T. L. *J. Phys. Chem. B* **2005**, *109*, 23618−23623. (h) Leung, B. O.; Read, D. L.; Armstrong, D. A.; Rauk, A. *J. Phys. Chem. A* **2004**, *108*, 2720−2725.

(14) (a) García-Melchor, M.; Pacheco, M. C.; Nájera, C.; Lledós, A.; Ujaque, G. *ACS Catal.* **2012**, *2*, 135−144. (b) Manzini, S.; Poater, A.; Nelson, D.; Cavallo, L.; Nolan, S. P. *Chem. Sci.* **2014**, *5*, 180−188. (c) Manzini, S.; Poater, A.; Nelson, D. J.; Cavallo, L.; Slawin, A. M. Z.; Nolan, S. P. *Angew. Chem., Int. Ed.* **2014**, *53*, 8995−8999.

(15) Martin, R. L.; Hay, P. J.; Pratt, L. R. *J. Phys. Chem. A* **1998**, *102*, 3565−3573.

(16) (a) Adlhart, C.; Hinderling, C.; Baumann, H.; Chen, P. *J. Am. Chem. Soc.* **2000**, *122*, 8204−8214. (b) Wang, H.; Metzger, J. O. *Organometallics* **2008**, *27*, 2761−2766. (c) Wang, H. Y.; Yim, W. L.; Guo, Y. L.; Metzger, J. O. *Organometallics* **2012**, *31*, 1627−1634.

(17) Chen, P.; Dougan, B. A.; Zhang, X. H.; Wu, Y. D.; Xue, Z. L. *Polyhedron* **2013**, *58*, 30−38.

(18) Jacobsen, H.; Cavallo, L. *ChemPhysChem* **2012**, *13*, 562−569.

(19) Haller, L. J. L.; Page, M. J.; Erhardt, S.; Macgregor, S. A.; Mahon, M. F.; Abu Naser, M.; Velez, A.; Whittlesey, M. K. *J. Am. Chem. Soc.* **2010**, *132*, 18408−18416.

(20) Grimme, S. *ChemPhysChem* **2012**, *13*, 1407−1409.

(21) The geometry optimizations with BP86-d3 and B3LYP-d3 failed in locating a barrier for **I→II** step, becoming a barrierless step, and to compare with the experimental data of 66 kJ/mol to describe the upper barrier the energy for **II→III** was used, anyway removing this value the MUE for G values for BP86-d3 and B3LYP-d3 were 4 and 3 kJ/mol larger, respectively.

(22) Yang, H.-C.; Huang, Y.-C.; Lan, Y.-K.; Luh, T.-Y.; Zhao, Y.; Truhlar, D. G. *Organometallics* **2011**, *30*, 4196−4200.

(23) (a) Hillier, I. H.; Pandian, S.; Percy, J. M.; Vincent, M. A. *Dalton Trans.* **2011**, *40*, 1061−1072. (b) Pandian, S.; Hillier, I. H.; Vincent, M. A.; Burton, N. A.; Ashworth, I. W.; Nelson, D. J.; Percyc, J. M.; Rinaudo, G. *Chem. Phys. Lett.* **2009**, *476*, 37−40.

(24) (a) Herbert, M. B.; Lan, Y.; Keitz, B. K.; Liu, P.; Endo, K.; Day, M. W.; Houk, K. N.; Grubbs, R. H. *J. Am. Chem. Soc.* **2012**, *134*, 7861−7866. (b) Miyazaki, H.; Herbert, M. B.; Liu, P.; Dong, X. F.; Xu, X. F.; Keitz, B. K.; Thay, U.; Mkrtumyan, G.; Houk, K. N.; Grubbs, R. H. *J. Am. Chem. Soc.* **2013**, *135*, 5848−5858.

(25) Thiel, V.; Hendann, M.; Wannowius, K. J.; Plenio, H. *J. Am. Chem. Soc.* **2012**, *134*, 1104−1114.

(26) Deshmukh, P. H.; Blechert, S. *Dalton Trans.* **2007**, *24*, 2479−2491.

(27) Nunez-Zarur, F.; Solans-Monfort, X.; Rodriguez-Santiago, L.; Sodupe, M. *Organometallics* **2012**, *31*, 4203−4215.